Hybrid-PIC Simulation of a Hall Thruster Plume on an Unstructured Grid with DSMC Collisions

Murat Celik*, Mark Santi*, Shannon Cheng*, Manuel Martinez-Sanchez**
Jaime Peraire**
Massachusetts Institute of Technology
Cambridge, MA, 02139
IEPC-03-134

Abstract

Although several operational codes are available for the prediction of plume dynamics of Hall thrusters and their interactions with spacecraft surfaces, their coverage of the range of physical phenomena involved and their ability to model complex geometries and material combinations has tended to be fairly restricted. We have initiated the development of a more comprehensive suite of models intended to be used either on their own, or as modules in an overall architecture of the type recently initiated at the Air Force Research Laboratory (Fife, et al. [1]). As a first stage in this development, the simplified physics currently embodied in an existing plume code (D. Oh, 1997 [2]) has been implemented in a new unstructured tetrahedral grid designed to couple with the surface grids generated by the AFRL for realistic representation of a typical spacecraft. A detailed source model that includes separate distributions for single and double ions as well as different populations has been integrated. More refinements on sputtering and material deposition and a method for predicting plasma behavior in non-quasineutral regions are planned, but have not yet been incorporated. The code models Xenon ions, double ions and neutrals kinetically, whereas the electrons are modeled as a fluid continuum. Direct Simulation Monte Carlo (DSMC) techniques are used to simulate the important collisions between kinetically modeled particles. Preliminary results presented here are compared to laboratory measurements on the plume of a low-power thruster.

Introduction

A major limitation of most previous work in Hall thruster plume simulation has been the lack of flexibility in using and comparing the different modeling techniques. Another area requiring improvement is the capability of a single code to accurately predict plume behavior in dissimilar environments. A new hybrid-PIC DSMC simulation (called AQUILA) is being developed to work within the Air Force Research Laboratory's COLISEUM framework that will provide modelers a vast number of options in computationally simulating the plume. The COLISEUM architecture allows users to run a variety of simulations at varying degrees of fidelity on the same platform while minimizing the overhead of changing methods [1]. The methodology implemented in AQUILA strives to allow the simulation of a Hall thruster plume in its entire operational regime, ranging from imperfect vacuum tank conditions to the actual in-space environment.

AQUILA includes many new aspects that expand the capabilities of Hall thruster plume simulations. The hybrid-PIC code has been implemented on a 3D unstructured grid that enables the modeling of complicated and realistic geometries. In order to ensure the proper plume expansion, a new source model divides the source particles into separate populations to accurately reproduce the particle distributions at the thruster exit plane. The DSMC collision model has been altered to account for particles with very different weightings to enable simulations with a background. Finally, results will demonstrate the progress in implementing the model and show comparisons to recent experimental data.

---

* Graduate Student, Department of Aeronautics & Astronautics
** Professor, Department of Aeronautics & Astronautics

Unstructured Grids

A 3D unstructured, tetrahedral mesh is now used in modeling the plume. Tetrahedra offer the most flexibility when creating the simulation grid because they can closely conform to any geometry. Grids are created using GridEx [3], a NASA Langley gridding package created for computational fluid dynamics. Solid models are read into GridEx using a parasolid format, after which two options are available for creating the 3D grid.

First, the surface and volume grid can both be created within GridEx. This option gives users the most control over how the grid is created because multiple sources can be specified to dictate grid refinement in particular areas of the computational domain. Sources can take the form of points, lines, or triangles as specified by the user. By entering certain values such as the desired tetrahedron edge length and distance to transition to the full grid size, the user has strong control over how the grid is created and can manipulate it to match with expected conditions within the plume. The second option for creating grids is more streamlined within COLISEUM, but has less control over the grid. COLISEUM currently contains the MGEN routines written by J. Peraire [4] that can generate the tetrahedral volume grid from a triangulated surface grid. These MGEN routines are the same ones used in GridEx, but there is currently no capability in COLISEUM for specifying sources within the domain. Thus, a commercial surface gridding program such as COSMOS can create the surface, then COLISEUM can read the output from that package and generate the 3D grid. This method offers the most flexibility to the user because any piece of software can be used to create the surface triangulation, but at the cost of decreased control over the growth of the volume grid.

AQUILA uses the standard finite element weighting formulation as found in [5] to interpolate properties over the domain. Linear basis functions are used, and weighting from the nodes is determined by the volume coordinates for the element. The basis functions can be simplified to a linear form,

$$N_i = \frac{\alpha_i + \beta_i x + \gamma_i y + \delta_i z}{6V} \tag{1}$$

where i corresponds to each of the four connected nodes for each tetrahedron. Thus, interpolating charges from the particles to the nodes and interpolating the calculated fields from the nodes back to the particle positions utilize the same linear relationships.

$$\rho_i = \sum_k q_k N_i(\underline{x}_k) \tag{2}$$

$$F_k = q_k \sum_i E_i N_i(\underline{x}_k) \tag{3}$$

where the subscript i represents mesh node properties and the subscript k represents particle properties. Using linear shape functions has the disadvantage that having piece-wise linear potential leads to piece-wise constant electric fields, possibly leading to tessellations in the fields as a particle moves through the domain. Quadratic basis functions are in the process of being implemented, which should provide better accuracy and stability.

The particle mover uses the same linear basis functions as the weighting formulation to determine the particle's element location. A leap-frog time marching algorithm is used to update the particles' position and velocity. When a particle changes element location, a directional search is performed by checking neighboring tetrahedra shape functions at the particle's new position.

The potential is currently being calculated by assuming quasi-neutrality and inverting Boltzmann's equation,

$$\phi = \phi_0 + \frac{kT_e}{e} \ln\left(\frac{n_e}{n_{e0}}\right) \tag{4}$$

where n_e is calculated by tracking the particles and weighting the charges to the grid nodes. A slightly more refined method of calculating potential is incorporated using a polytropic relationship between electron temperature and density,

$$\frac{T_e}{T_{e0}} = \left(\frac{n_e}{n_{e0}}\right)^{n-1} \tag{5}$$

where n is about halfway between the isentropic n = γ = 5/3 and the isothermal n = 1. Integration of the momentum balance $\nabla(n_e k T_e) = e n_e \nabla\phi$ with $\frac{\nabla T_e}{T_e} << \frac{\nabla n_e}{n_e}$ leads to

$$\phi = \phi_0 - \frac{kT_{e0}}{e}\frac{1-\left(\frac{n_e}{n_{e0}}\right)^{n-1}}{n-1} \tag{6}$$

Both formulations assume quasi-neutrality throughout the domain, but the latter allows for a simple variation in the electron temperature in the plume. Once the potentials have been calculated, the electric field is found from the divergence, and the particles are moved.

Source Model

The source model represents the state of the plasma exiting the Hall thruster and must be detailed if accurate results of its expansion as a plume are desired. For this work, the BHT-200 is simulated, as experimental data of its operation in a vacuum tank is available for comparison. The thruster's exit plane distributions are generated using *HPHall*, a 2D hybrid-PIC engine code written by M. Fife [6]. The present source model is an improvement over that used in [7] since an upgraded version of *HPHall* treats single and double ions separately, thus eliminating the assumption that the two ion species share the same distribution. Figure 1 shows the computational grid with the thruster exit and exit plane.

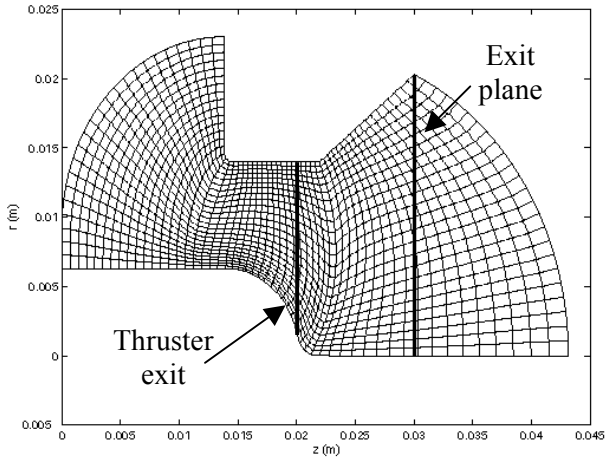

Figure 1. BHT-200 computational geometry.

The exit plane is chosen at a distance of 0.30 m from the back of the ionization channel as the space potential has mostly fallen off by the time ions reach this axial position. The plume code does not directly model ions falling through the potential produced by the thruster, so it is important that these effects are already incorporated into the source model. The exit plane is divided into 25 radial bins which in turn are sub-divided into axial and radial velocity bins. As particles cross the plane, single and double ion data are recorded separately so that distinct distributions for each species can be derived. Figures 2 and 3 show the axial and radial velocity distributions of single ions at each radial bin. The vertical line in each plot marks the average velocity for that radius. Two distinct peaks are observed in the radial velocity distributions close

to the thruster centerline. This phenomenon is attributed to the fact that as particles in *HPHall* cross the centerline grid boundary, they are reflected in order to represent particles coming from the opposite side of the annular engine. It is clear that the calculated average velocity values for the radial component do not accurately reflect these two distinct populations of ions. Thus, the source model incorporates distributions to represent particles reflected at the centerline and particles originating from the main engine channel independently.

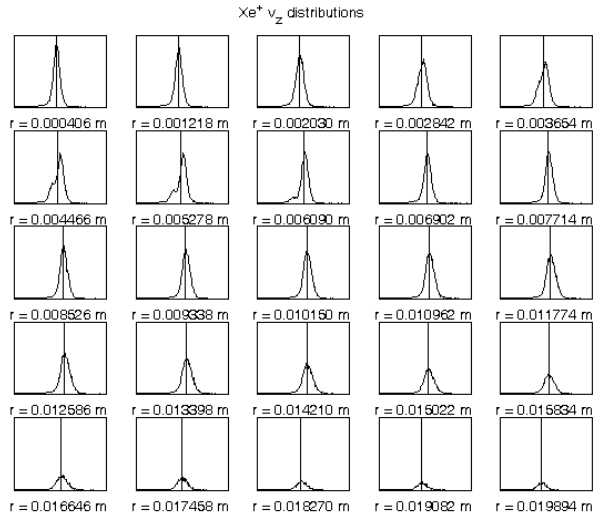

Figure 2. Xenon single ion axial velocity distributions. Horizontal axes are axial velocity, v_z, ranging from 0 to 35,000 m/s. Vertical axes are number of Xe^+ ranging from 0 to $3x10^{12}$.

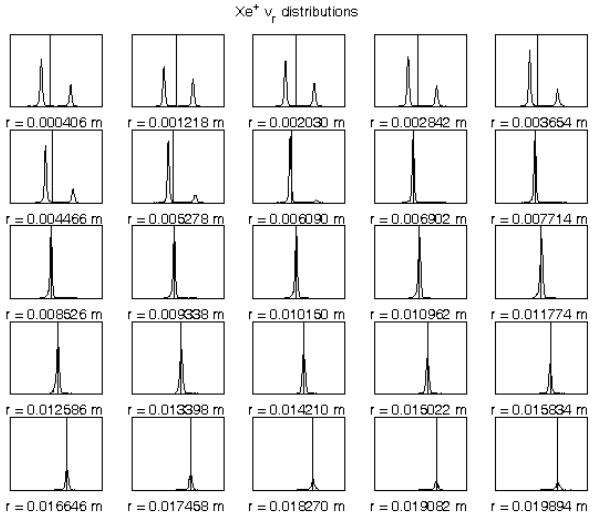

Figure 3. Xenon single ion radial velocity distributions. Horizontal axes are radial velocity, v_r, ranging from –35,000 m/s to 35,000 m/s. Vertical axes are number of Xe^+ ranging from 0 to $4x10^{12}$.

The flux as a function of radial position from the thruster centerline is divided by the corresponding velocity magnitude to obtain a number density distribution. From this, a cumulative distribution function is computed and used to inject source particles into the simulation domain with the correct radial distribution. For values below r = 0.00714 m, the ion may either be part of the aforementioned near-side or far-side populations. Particles inserted in this range are proportionally assigned to each population based on the fractional amount of far-side ions at each radial position computed from *HPHall* results. Once location and population are assigned to a particle, axial and radial velocities are also assigned as a function of radial position. Figures 4 and 5 depict the average velocity distributions for the near-side population single and double ions.

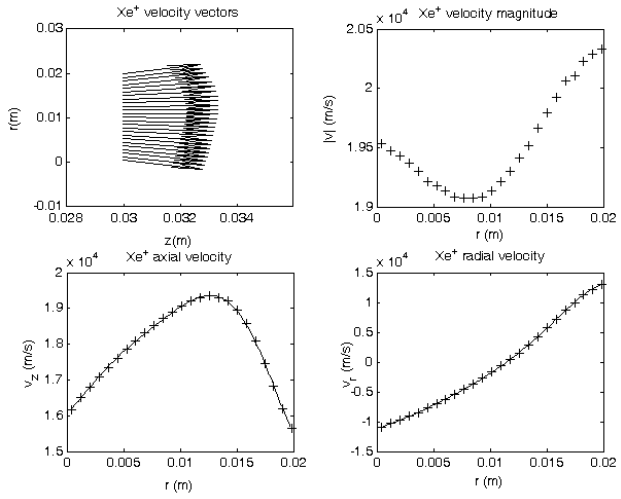

Figure 4. Single ion near-side population velocity distributions.

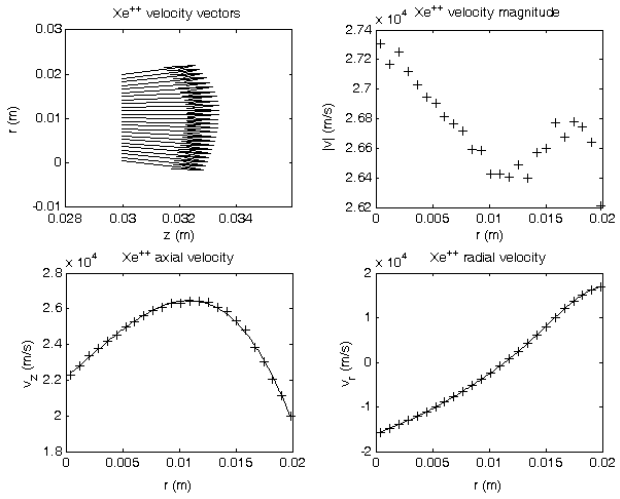

Figure 5. Double ion near-side population velocity distributions.

The velocity magnitude shows the double ions as having about 1.3 times the velocity, or slightly less than double the energy of the single ions. Double ions are formed throughout the acceleration channel and thus fall through a larger range of potentials than the single ions. The two velocity components are sufficient to provide the particles with the proper divergence angle. The point where the radial velocity distributions transition from positive to negative values is ~0.01 m, corresponding to the center of the channel. Thus, the proper beam dispersion is achieved. The axial velocity distributions have a noticeable spread, so Gaussian fits are done at each radius to determine an average axial ion temperature which is incorporated into the model by adding a thermal component to the axial velocity. The radial velocity distributions are narrow enough that no radial ion temperature is assumed. This approximation may need revision later.

The same procedure is used to model the far-side populations. Details of these calculations, as well as information about additional parameters used in specifying the source model can be found in [8].

Collision Dynamics

Despite the low density of particles in the plume region, according to experimental results, momentum-exchange (elastic) and charge-exchange (CEX) collisions have a profound effect on the Hall thruster plume structure. Especially for vacuum tank testing cases, the high density of the background neutrals increases the rate of charge-exchange collisions between the thruster ions and the vacuum tank neutrals, causing the spread of plume ions to the backfield region. For simulations of the vacuum chamber, background neutrals are initialized assuming the ideal gas law based on the temperature and pressure conditions of the chamber during testing.

In the AQUILA collision model, the most important momentum-exchange and charge-exchange collisions are modeled. The elastic collisions modeled are Xe-Xe, Xe-Xe^{+} and Xe-Xe^{++}. Additionally, Xe-Xe^{+} and Xe-Xe^{++} CEX collisions are also modeled. Only binary collisions are considered.

CEX Collisions

Charge-exchange collisions occur when a highly energetic ion collides with a neutral with a much slower speed (i.e. neutral thermal speed). As a result of this reaction, a slow ion and a fast neutral are created. The charge-exchange collisions are simulated by exchanging electrons between the colliding particles and maintaining the pre-collision particle velocities. Physically, there would be a momentum change during a charge-exchange collision, but conventionally, CEX collisions approach the zero-momentum exchange limit of elastic scattering collisions.

At the near plume region, close to the thruster exit plane, the ions accelerate electrostatically through the potential gradient, but the neutrals remain unaffected by the potential field. Due to their high velocities, the trajectories of fast ions emitted from the thruster are relatively unaffected by the field, thus expanding into the plume with a narrow divergence angle. When these fast ions have CEX collisions with the slow neutrals in front of the thruster, they exchange electrons, thus transforming the slow neutrals into slow ions. These slow ions respond strongly to the electric field in the near plume region and are pulled behind the thruster more easily. This effect causes spreading in the plume, and the resulting trajectories of the CEX ions make them more likely to interact with the spacecraft components.

In this model, for CEX collisions between Xe-neutral and Xe^{+}, the following cross section measured by Pullins, et al. [9] is adopted,

$$\sigma_{Xe-Xe+}(g) = (-23.3 \times \log_{10}(g) + 188.81) \times 1.1872 \times 10^{-20}\, m^2 \qquad (7)$$

where g is the relative velocity. The remaining CEX cross-section is the same as that used by Oh [2].

Elastic Collisions

Elastic collisions involve the exchange of momentum between the colliding particles. Due to high ionization rates for Hall thrusters (on the order of 90%), the number of neutrals leaving the thruster is low. However, the thruster neutrals move with much slower speeds compared to the thruster ions, resulting in comparable neutral and ion densities at the thruster exit plane. This increases the importance of elastic collisions between ions and neutrals and elastic collisions between neutrals. Moreover, for vacuum chamber testing cases, the high density of background neutrals increases the elastic collision rate dramatically. Elastic collisions between neutral Xenon atoms and Xe, Xe^{+} Xe^{++} are modeled, but due to the low densities and low cross-section for the Xe^{+}-Xe^{++} elastic collisions, these types of collisions are not modeled at this stage.

In this model, the elastic collision cross-sections, as well as the method for calculating the scattering angle distributions, are the same as those discussed by Oh [2].

NTC-DSMC

The No-Time-Counter (NTC) DSMC method of Bird [10] is used to simulate the collision effects in the plume region. Collections of real particles are grouped into macroparticles, which lie in the computational volume. In AQUILA, both DSMC and PIC use the same tetrahedral grid. Particle pairs coexisting in one computational cell are candidates for collisions during each time step. Depending on the number of particles in a cell, the number of pairs of each collision type is determined. Until this predetermined number is reached, pairs are randomly selected, and the collision probability of the selected pair is then calculated using the product of the pair's relative velocity and the respective collision cross-section. The determined probability is compared with a random fraction between 0 and 1 to decide the likelihood of the collision occurring. If the collision occurs, then the appropriate collision dynamics are performed, and the properties (i.e. velocity components) of the colliding particles are changed accordingly. After all the predetermined number of pairs have been selected and the collisions are performed, the process of performing the collisions in the next computational cell is started. The process is repeated for every cell at every time step.

Pair Selection Scheme

Assuming that particles of species p and q are located in a box of volume V and have number densities n_p and n_q respectively, the expected number of real collisions happening in a time interval Δt is given by the expression,

$$n_p n_q \overline{\sigma_T g} V \Delta t \tag{8}$$

where σ_T is the total collision cross-section, g is the relative velocity, and $\overline{\sigma_T g}$ represents the mean value of $\sigma_T g$ for all possible pairs.

If the simulation macroparticles represent W_p and W_q real particles for the p and q species, respectively, then the number densities are given by $n_p = N_p W_p / V$ and $n_q = N_q W_q / V$, where N represents the number of simulation particles within the given cell volume, and W is the weighting factor for the species. If $W_p > W_q$, then the expected number of numerical collisions in a time interval Δt is given by,

$$N_p N_q W_p \overline{\sigma_T g} \Delta t / V \tag{9}$$

where $W_p \overline{\sigma_T g} \Delta t / V$ corresponds to the mean collision probability, $\overline{P}$, of all possible pairs. In order to perform the correct number of collisions, every possible combination could be selected and collisions could be performed based on the selected pair's collision probability, P=$W_p \sigma_T g \Delta t / V$. However, this would require $N_p N_q$ pairs to be selected, of which most would be rejected due to a low collision probability. For the cases where $N_p N_q >> 1$ and $P << 1$, this would be a very computationally intensive process. This problem can be solved if only a fraction of the possible pairs are selected, while being accepted for collisions with a correspondingly higher probability. To accomplish this, assume that instead of selecting $N_p N_q$ pairs,

only $N_p N_q/F$ pairs are selected, and the collision probability of each selected pair is increased from P to $F \times P$, where F is a factor greater than 1. This process can be made more efficient as F becomes larger. In the limiting case, $F \times P \leq 1$ gives $F=1/P_{max}$. Thus, this gives

$$F \times P = \frac{P}{P_{\max}} = \frac{\sigma_T g}{(\sigma_T g)_{\max}} \tag{10}$$

for the new collision probability of the selected pair. For a large number of iterations, this process on average gives the expected number of collisions per time step. As discussed above, after a fraction $(1/P_{max})$ of the possible pairs are selected, the collision probability, $\sigma_T g /(\sigma_T g)_{\max}$, of each selected pair is compared with a random fraction R. If the pair's collision probability is greater than R, then the pair is selected, the appropriate collision dynamics are performed, and the properties of the colliding particles are changed accordingly. If the probability is less than R, then the pair is rejected and a new pair is selected. The $(\sigma_T g)_{\max}$ value is stored for each collision type and updated as a new maximum is encountered.

Handling of different weighting factors

If the weighting factors are different for the colliding macroparticles, a simulated collision might represent W_p particles of species p colliding with W_q of species q. In the following discussion, the weighting factor for the particles of species p, W_p, is considered to be larger than the weighting factor for the particles of species q, W_q (i.e. $W_p > W_q$). After performing the appropriate collision dynamics for a pair selected for collision, the properties (i.e. velocity components) of the lower weight particle are always changed to the post-collision values, but the properties of the higher weight particle are changed to post-collision values with a probability of W_q/W_p. With this method, the momentum might not be conserved for individual collisions, but cumulative momentum will be conserved for a large number of collisions. This also explains why Equation 9 has the higher weighting factor, W_p.

Surface Interactions

Various surface interaction capabilities are available in AQUILA, and the desired material interactions can be specified by the user. Options available include reflection, absorption, accommodation, and sputtering. In addition to the sputtering models previously available, the modified Yamamura method for sputtering yield described in [7] and [8], as well as the outgoing angular distribution, have been added to COLISEUM. Sputtered particles are created and their deposition is recorded by tracking them through the simulation, assuming straight-line trajectories.

Results

For the purposes of preliminary testing and comparison to experiments conducted in our laboratory by Y. Azziz [11], simulations are performed on the grid seen in Figures 6 and 7, mimicking the vacuum chamber at MIT. Both the surface and the volume grids are generated with GridEx, and a grid line source is placed from the front face of the thruster out to 25cm to obtain better grid refinement in the dense plasma region at the thruster exit.

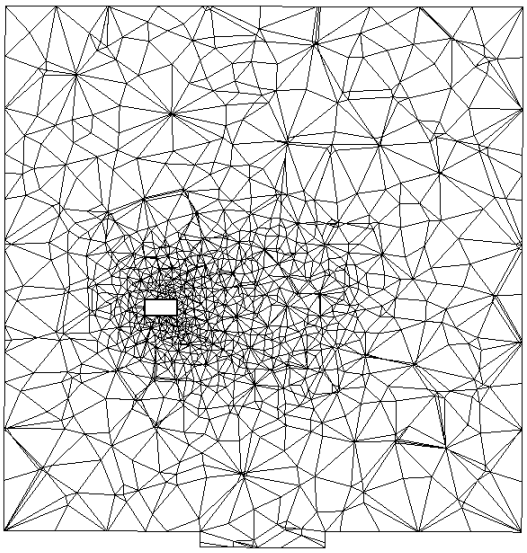

Figure 6. Cross-section of simulation grid.

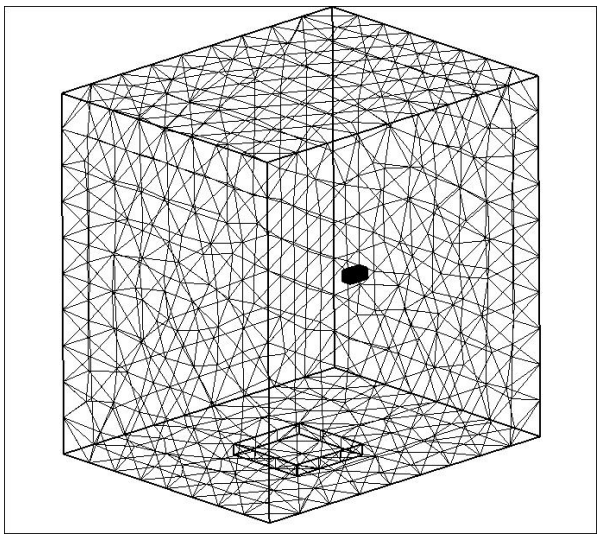

Figure 7. 3D view of simulation grid.

The vacuum tank pressure of 2.6×10^{-5} Torr is simulated with a corresponding background neutral density at 300K that is maintained by reflecting neutrals with 65% accommodation as they strike simulated walls. Ions are deleted upon impact with the walls. The thruster uses the source model described above and injects particles at a mass flow rate of 0.70 mg/s and a beam current of 0.4022 A. Cases considering a constant electron temperature of 2eV as well as the polytropic case with n = 1.25 and T_{e0} = 2.8eV imposed along the centerline at r = 25cm are run until steady-state behavior is achieved. Simulated results of current density and plasma potential are compared to experimental results.

Ion Current Density

The angular profile of the ion current density is sampled at a radial distance of 25 cm from the thruster exit plane. Figure 8 compares results with the profiles measured for the BHT-200 thruster in the MIT-SPL vacuum chamber.

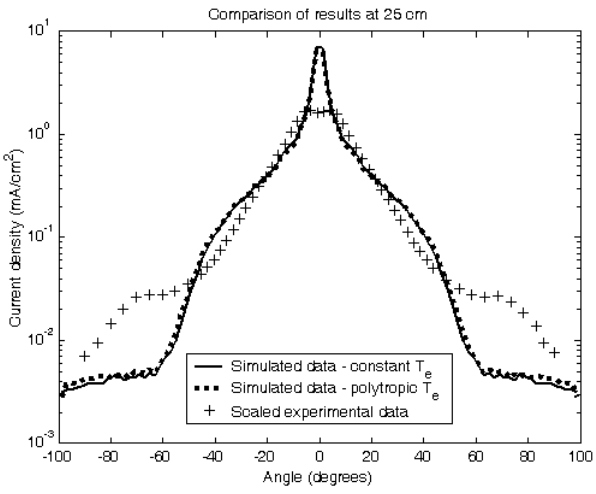

Figure 8. Comparison of current density results at 25 cm.

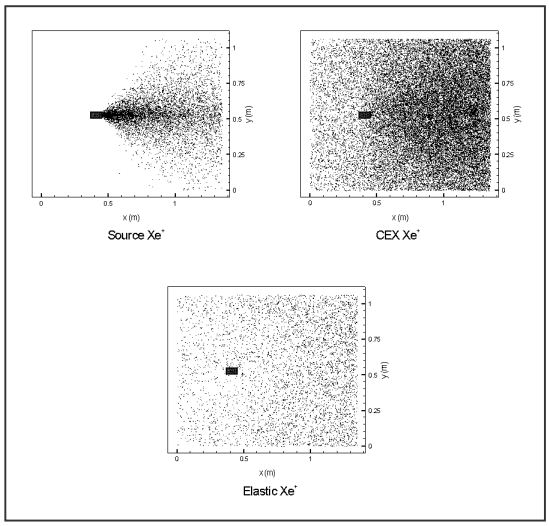

Figure 9. Scatter plots of different single ion populations.

In the simulation profiles, the ion current density in the angle range of –5 to 5 degrees is much larger than the measured current density. This might be a result of the source model predicting too little angular spread about the axial direction. Between 10 and 50 degrees, the results of the computation match the measured flux well. This constitutes partial validation of the source model, since that region is dominated by primary ions. However, between 50 and 90 degrees, where CEX ions are expected to dominate, the calculation significantly underpredicts the data. Figure 9 shows that the CEX ions do not significantly cluster about the 60-90° angular range, as should be expected. This may be an indication of deficiencies in the modeling of the region of CEX generation, i.e., the initial 10 cm of the plume. In this physically complex region, the one-to-one connection between electron number density and potential is likely to break down, and stronger radial fields may be present. As Figure 8 shows, the constant temperature model and the polytropic model do not differ greatly as far as predicting the ion flux distributions.

Comparison to results in [8], which used a completely different collision model and grid, show very little difference, except for a smoother merging of the primary and CEX-dominated regions in the present calculation.

Plume Plasma Potential

The potential probe data gives the strongest confirmation that the code is accurately modeling the physics of the plume. The computational results represent a simulated time-averaged probe at 25 cm from the center of the thruster face spanning an arc of 180°. As seen in Figure 10, both the constant and polytropic electron temperature measurements correspond closely to the experiment. The total potential drop between the centerline and the wings is approximately 7 V for both the experiment and the simulations. Although certain regions do not match exactly with the measured data, the strong correlation provides confidence that the computational model can provide a reasonable approximation of the plume expansion.

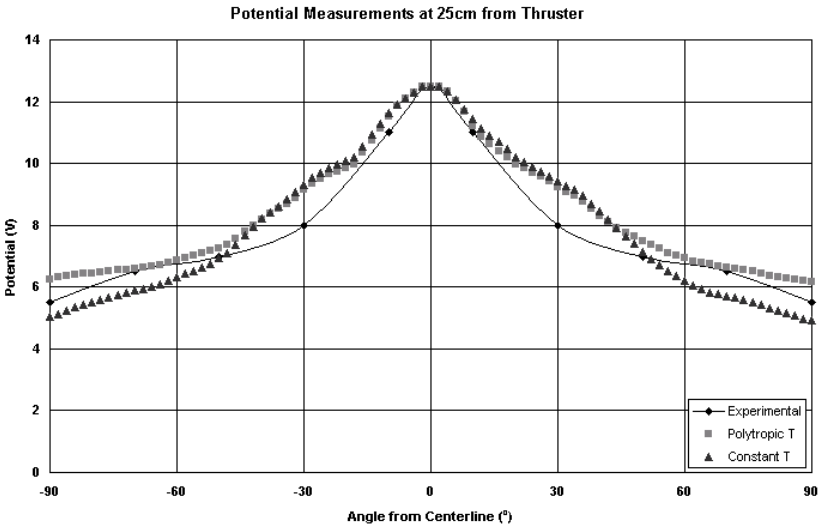

Figure 10. Comparison of potential results at 25 cm.

Conclusions

The initial development and integration of AQUILA into the COLISEUM architecture has been successful. Although many areas of the code still require improvement and validation, preliminary results indicate AQUILA's potential to provide insight into plume dynamics. Now that a framework has been put in place, attention can be focused on investigating inaccuracies in the modeling assumptions, enhancing capabilities, as well as utilizing and building upon its strengths.

References

[1] Fife, J. M. et al., "The Development of a Flexible, Usable Plasma Interaction Modeling System," AIAA-2002-4267, 38th AIAA/ASME/SAE/ASEE Joint Propulsion Conference, Indianapolis, Indiana, 2002.

[2] Oh, D. Y., *Computational Modeling of Expanding Plasma Plumes in Space Using a PIC-DSMC Algorithm*, PhD thesis, Massachusetts Institute of Technology, February 1997.

[3] Jones, W. T., "An Open Framework for Unstructured Grid Generation," AIAA-2002-3192, 32nd AIAA Fluid Dynamics Conference and Exhibit, St. Louis, Missouri, 2002.

[4] Peraire, J., and K. Morgan, "Unstructured Mesh Generation for 3D Viscous Flow," AIAA-1998-3010, AIAA 16th Applied Aerodynamics (APA) Conference, Albuquerque, New Mexico, June 1998.

[5] Zienkiewicz, O.C., and R. L. Taylor, *The Finite Element Method*, Volume 1, Butterworth-Heinemann, Oxford, 2000.

[6] Fife, J. M., *Hybrid-PIC Modeling and Electrostatic Probe Survey of Hall Thrusters*, PhD thesis, Massachusetts Institute of Technology, September 1998.

[7] Cheng, S. Y., and M. Martinez-Sanchez, "Simulations for a Shuttle-based Hall Thruster Plume Experiment," 27th International Electric Propulsion Conference, Pasadena, CA, October 2001.

[8] Cheng, S. Y., *Computational Modeling of a Hall Thruster Plasma Plume in a Vacuum Tank*, SM thesis, Massachusetts Institute of Technology, February 2002.

[9] Pullins, et al., "Ion Dynamics in Hall Effect and Ion Thrusters: $Xe^+ + Xe$ Symmetric Charge Transfer," AIAA-2000-0603, 38th Aerospace Sciences Meeting and Exhibit, Reno, Nevada, 10-13 January 2000.

[10] Bird, G.A. *Molecular Gas Dynamics and the Direct Simulation of Gas Flows*, Oxford University Press, Oxford, 1994.

[11] Azziz, Y., and M. Martinez-Sanchez, "Plasma Measurements on a 200-Watt Hall Thruster Plume," IEPC-03-140, 28th International Electric Propulsion Conference, Toulouse, France, March 2003.